ISSN 1573-160X, *PHYSICAL OCEANOGRAPHY*, Vol. 33, Iss. 2, pp. 281-306 (2026)

published in *Morskoy Gidrofizicheskiy Zhurnal*, 2026, Vol. 42, Iss. 2, pp. 263–274

Original article

Features of the Response of Level Fields and Currents in the System of the North and Baltic Seas to Atmospheric Forcing during the Formation of Major Baltic Inflow

E. A. Zakharchuk [1] ✉, **N. A. Tikhonova** [1, 2], **V. N. Sukhachev** [1, 2]

[1] *St. Petersburg State University, Saint Petersburg, Russian Federation*
[2] *N. N. Zubov State Oceanographic Institute, Rosgidromet, Moscow, Russian Federation*
✉ *eazakharchuk@yandex.ru*

Abstract

Purpose. The purpose of the work is to study the features of the response of sea level fields and currents in the system of the North and Baltic Seas to the impact of changes in atmospheric pressure and tangential wind stress during the formation of the Major Baltic Inflow in 2014, based on reanalysis data on meteorological and hydrophysical fields, as well as numerical experiments using a three-dimensional baroclinic hydrodynamic model.

Methods and Results. To achieve the stated goal, the following procedures were performed: decomposition of hydrometeorological fields into complex natural orthogonal functions; cross-correlation and cross-wavelet analysis between the main components of field decomposition; spectral, cross-correlation and cross-spectral analysis of current oscillations and tangential wind stress; free level oscillations were modeled, and their spectral structure was compared with the spectra of current oscillations during a large inflow.

Conclusions. During the formation and propagation of the Major Baltic Inflow in 2014, the main energy transfer from the baric formations to the movement of water masses took place in the range of several weeks, while in a year without an inflow, it occurred in the range of several days. During the large inflow, the water mass response to the impact of anemobaric forces occurred in the form of low-frequency wave processes, which had the signs of progressive and standing modes of wave motion. The analysis both of the synoptic situation over the North Atlantic and the results of numerical hydrodynamic modeling of free level fluctuations in the system of the North and Baltic Seas has shown that the largest sea level gradients between the Kattegat Strait and the southwestern Baltic, as well as the highest current velocities in the Danish Straits, were observed during the Major Baltic Inflow on December 11, 2014, when the movement of a deep atmospheric cyclone slowed down sharply to 1.0 m/s, and its speed became equal to the phase velocities of free low-frequency waves in the North and Baltic Seas. This fact makes it possible to further investigate the hypothesis about the resonance mechanism for the generation of Major Baltic Inflows.

Keywords: Major Baltic inflow, Baltic Sea, North Sea, Danish Straits, sea level fluctuations, currents, numerical hydrodynamic modeling, reanalysis, statistical analysis, cross-wavelet analysis

Acknowledgements: The study was carried out with the financial support of the RSF grant No. 24-27-00412 “Clarifying the mechanisms of generation and non-stationarity of the Major Baltic inflows” https://rscf.ru/project/24-27-00412/.

For citation: Zakharchuk, E.A., Tikhonova, N.A. and Sukhachev, V.N., 2026. Features of the Response of Level Fields and Currents in the System of the North and Baltic Seas to Atmospheric Forcing during the Formation of Major Baltic Inflow. *Physical Oceanography*, 33(2), pp. 281-306.

Introduction

Major Baltic Inflows (MBI) are irregular intrusions into the Baltic Sea of extremely large volumes of saline, oxygen-rich North Sea waters, reaching 90–258 km^3 and lasting 6–29 days. These waters penetrate into the deep-water areas of the open Baltic, exerting a beneficial impact on the ecological state of this sea [1–7]. The study of MBIs dates back to the end of the 19th century, when light vessels began operating in the Danish Straits and other areas of the Baltic Sea, conducting instrumental measurements of temperature, salinity, and currents [1] [2]. Further development of oceanographic research in the Baltic and North Seas region has provided extensive information on the variability of meteorological processes during the formation and propagation of MBIs, their statistical characteristics, vertical structure, transformation features, and propagation pathways in the Baltic Sea [2] [1–13].

According to historical data, most researchers explain the causes of MBIs by the Ekman mechanism, which contributes to the formation of wind-driven currents and associated setup/setdown sea level oscillations in the North and Baltic Seas system [1–5, 8, 14–16]. A key precursor of an MBI is considered to be prolonged easterly winds, which cause water outflow from the Baltic to the North Sea and lower its level and the sea level in the south of the Kattegat Strait. This pre-inflow period, lasting 1–3 weeks [4, 5, 11], is very important for the formation of a future MBI because the longer and more intense the outflow from the Baltic, the more its level drops and the greater the level gradient that forms between the Kattegat and the southwestern Baltic before the MBI begins, which largely determines the MBI intensity [4, 5, 9].

Then meteorological conditions change: the easterly wind weakens and begins to shift to a westerly one; as a result, the sea level in the Kattegat Strait starts to rise, gradually approaching the level in the southwestern Baltic [4, 5, 9].

The main inflow phase begins when the water level rise in the North Sea and the Kattegat Strait, which started earlier, reaches a critical value. This creates a level gradient directed from the Kattegat to the southwestern Baltic, which continues to increase under the influence of persistent westerly winds lasting two to three weeks. At the same time, westerly winds cause a setdown in the Danish Straits area, creating a level difference between the Kattegat and the southwestern Baltic reaching 1.0–1.7 m [10, 17, 18]. This leads to intensive transport of highly saline, oxygen-rich waters from the North Sea to the Baltic, which subsequently causes a level decrease in the North Sea and an increase in the Baltic [4, 5, 9].

The inflow ends when the westerly winds weaken, stopping the accumulation of North Sea waters in the straits. Since by this time the Baltic Sea level becomes higher than the North Sea level, an outflow from the Baltic to the North Sea begins;

[1] Svansson, A., 1975. *Physical and Chemical Oceanography of the Skagerrak and the Kattegat: Open Sea Conditions*. Fishery Board of Sweden, Institute for Marine Research. Report No. 1, 88 p.

[2] Antonov, A.E., 1987. [*Large-Scale Variability of the Hydrometeorological Regime of the Baltic Sea and Its Impact on Fishing*]. Leningrad: Gidrometeoizdat, 247 p. (in Russian).

this leads to a gradual return of the Baltic level to its mean value [4, 7, 9, 11]. However, to verify the Ekman mechanism, the cited works did not assess the features of the vertical structure of currents and the statistical relationships between the variability of tangential wind stress and currents in the North and Baltic Seas system during MBIs.

The authors of [1, 19] hypothesized that a positive salinity anomaly in the deep layers of the Kattegat Strait is a necessary condition for an intense inflow. However, subsequent studies showed that both positive and negative salinity anomalies were observed in the Kattegat before major inflows [20].

Analysis of two-dimensional probability distributions of wind velocity vectors in the North Sea during the formation of three MBIs (1983, 1993, 2003) indicated that the most frequent wind speeds during MBIs were 12–19 m/s, and directions ranged from southeast to west-northwest [7]. Further analysis revealed that in the period 1979–2010, cases with such wind conditions were 20 times more numerous than the MBIs themselves [7]. This result indicates that the Ekman mechanism of storm surge is not the only one responsible for MBI generation. Indeed, analysis of satellite altimetric data revealed a characteristic wave structure of water mass dynamics in the North and Baltic Seas during MBI formation [17]. Low-frequency wave processes with periods of 14–36 days were observed in these seas, propagating with an eastward component of phase velocity along isobaths. These waves were identified as barotropic topographic Rossby waves [17].

In [6], based on satellite altimetry data analysis, low-frequency waves in the sea level field during MBIs were identified as baroclinic topographic Rossby waves. Based on the analysis of meteorological information, a hypothesis about a resonant-wave mechanism for the generation of MBIs was proposed [6, 17]. However, this hypothesis has not been methodologically confirmed. In particular, the frequency-selective properties of the basin in the North and Baltic Seas system for identifying resonant frequencies were not investigated, nor were the values of cross-spectral density, coherence, and phase difference between anemobaric forces and current oscillations during MBIs estimated. Furthermore, the weekly discreteness and very coarse spatial resolution ($0.33 \times 0.33°$) of the satellite altimetry data array used do not guarantee complete reliability of the results obtained, especially for the region of narrow straits between the North and Baltic Seas. These doubts were confirmed in [21], which compared various statistical characteristics of synoptic sea level oscillations in the Baltic Sea between tide gauge and satellite altimetric data with improved daily discreteness and spatial resolution of $0.25 \times 0.25°$. It showed that altimetric data poorly describe oscillations with periods from several days to 3 weeks – precisely the period range in which MBIs are generated. Particularly poor agreement between tide gauge and satellite altimetric data was observed in the Danish Straits [21]. Also, methodological shortcomings in studying the wave mechanism of MBIs in the above-cited works include ignoring the influence of standing modes of low-frequency waves on the spatiotemporal variability of sea level fields in the Baltic and North Seas system during MBI events. These seas are significantly confined

marine basins, in which, according to theoretical concepts, standing modes of gradient-vortex and low-frequency gravity waves should be generated [22, 23].

After 1983, MBI events became much rarer, and the interval between them increased to 10–11 years [4, 6, 7, 9, 17]. The mechanism for such a significant reduction in the number of MBIs remains unclear. In [24], using numerical hydrodynamic forecasting, it was shown that in the current century, the reduction in barotropic MBIs will continue due to strengthening westerly winds, and the number of baroclinic inflows will decrease due to shorter periods of weak winds. However, analysis of instrumental wind measurements at coastal meteorological stations in the Baltic and North Seas region shows that in recent decades, there has been a decrease in the mean, variance, and maxima of wind, which is associated with a decrease in the intensity of atmospheric cyclogenesis [7, 25]. Results of numerical modeling using climate models indicate significant changes in cyclogenesis characteristics: starting from the end of the 20th century, in the cold season (October–March), there is a steady tendency toward a decrease in the frequency of atmospheric cyclones and a reduction in their intensity. According to forecasts, this trend will intensify throughout the 21st century [26].

The main purpose of this work is to assess, based on reanalysis data on meteorological and hydrophysical fields as well as numerical experiments with a three-dimensional baroclinic hydrodynamic model, the features of the response of sea level fields and currents in the North and Baltic Seas system to changes in atmospheric pressure and tangential wind stress during the formation of the 2014 MBI, and to compare the results obtained with similar estimates for the autumn-winter period of 2006, when no MBI was recorded.

Data and methods

The following hydrometeorological information archives were used:

– meteorological parameters from the ERA5 reanalysis, including wind speed and direction at a height of 10 m, as well as surface atmospheric pressure with a spatial resolution of $0.25 \times 0.25°$ for the period 1993–2022 (https://doi.org/10.24381/cds.adbb2d47);

– GLORYS12V1 hydrophysical field reanalysis data [3]. The GLORYS12V1 product is a global ocean eddy-resolving reanalysis (horizontal resolution 1/12°, 50 vertical levels) developed on the basis of the Copernicus Marine Environment Monitoring Service (CMEMS) global forecasting system operating in real time. The reanalysis is implemented based on the Nucleus for European Modeling of the Ocean (NEMO) numerical hydrodynamic model [27, 28] with assimilation of *in situ* and satellite data using an algorithm based on a variant of the Kalman filter. The assimilated variables in the NEMO model included altimetric data of sea level anomalies along satellite tracks, satellite data on sea surface temperature and sea ice concentration, as well as shipborne measurements of vertical profiles of seawater temperature and salinity.

[3] Drévillon, M., Lellouche, J.-M., Régnier, C., Garric, G. and Bricaud, C., 2023. *Quality Information Document for Global Ocean Reanalysis Products GLOBAL-REANALYSIS-PHY-001-030*. Technical Report. Copernicus Marine Environment Monitoring Service, 53 p.

Numerical modeling of oceanological fields using the INMOM model. To study the variability of oceanological processes during the formation and propagation of the 2014 MBI, as well as to analyze free oscillations of sea level in the North and Baltic Seas system, a three-dimensional nonlinear baroclinic hydrodynamic model was applied. This model is based on the sigma-coordinate model of marine circulation developed at the Institute of Numerical Mathematics of the Russian Academy of Sciences and known in the world scientific community as INMOM (Institute of Numerical Mathematics Ocean Model) [29, 30].

The INMOM model is based on the full system of nonlinear primitive equations of ocean hydrodynamics in spherical coordinates, taking into account the hydrostatic and Boussinesq approximations. We use the dimensionless quantity $\sigma = (z - \zeta) / (H - \zeta)$ as a vertical coordinate, where z is the standard vertical coordinate; $\zeta = \zeta(\lambda, \varphi, t)$ is the sea level deviation from the undisturbed surface (depending on longitude λ, latitude φ, and time t); $H = H(\lambda, \varphi)$ is the sea depth. The model uses 20 vertical sigma layers.

The prognostic variables are the horizontal velocity components, potential temperature, salinity, and sea level deviation from the undisturbed surface. Density is calculated using an equation of state that accounts for seawater compressibility and is adapted for numerical modeling [31].

The model also includes a sea ice thermodynamics module [32], consisting of three submodules:

– a thermodynamic module describing the processes of ice formation, melting, and snow accumulation;

– a dynamic module calculating ice drift velocities [4];

– an ice transport module modeling the evolution of ice and snow cover as a result of drift [33].

The modeling domain has a spherical grid with two poles, one located on the Jutland Peninsula (Denmark) and the other in southern Sweden (Fig. 1).

The spatial resolution of grid nodes in the area of the Danish Straits is about 300–700 m and proportionally increases to 4–6 km away from the straits.

Initial thermohaline fields (temperature and salinity) were taken from climatic data for January 2014 with a horizontal resolution of 4.5 × 9 km and a vertical step of 5 m, provided by the Copernicus Marine Service (http://marine.copernicus.eu).

Boundary conditions at the sea surface in the INMOM model were set using meteorological data from the ERA5 reanalysis [34]. The following parameters were used with a temporal resolution of 3 hours, a spatial step of 0.25°, and a coverage period from January 2014 to December 2015:

– air temperature and humidity at a height of 2 m;

– sea level pressure;

– wind speed at a height of 10 m;

– shortwave and longwave radiation fluxes;

[4] Briegleb, B.P., Bitz, C., Hunke, E., Lipscombe, W., Holland, M.M., Schramm, J. and Moritz, R., 2004. *Scientific Description of the Sea Ice Component in the Community Climate System Model, Version Three*. NCAR Technical Note TN-463+STR, NTIS #PB2004-106574. Colorado, Boulder: National Center for Atmospheric Research, 75 p. https://doi.org/10.5065/D6HH6H1P

– atmospheric precipitation amount.

At the liquid boundary (Fig. 1), the following were prescribed:

– monthly mean values of water temperature and salinity for 2014–2015;

– amplitudes and phases of 8 major tidal harmonics (M_2, S_2, N_2, K_2, K_1, O_1, P_1, M_4) obtained from the global tidal model TPXO (https://www.tpxo.net/global).

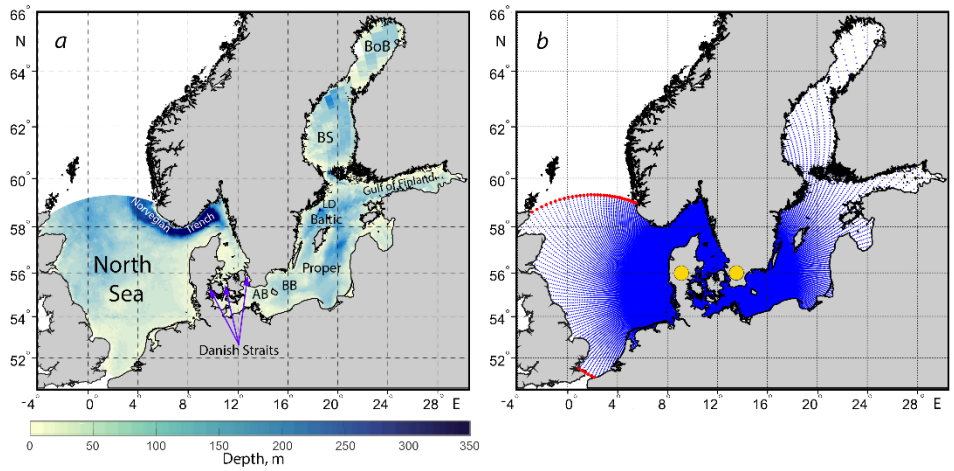

F i g. 1. Study region with bathymetry (*a*) and the grid area of the INMOM model (*b*). The red dotted line indicates the model liquid boundaries, and the yellow circles indicate the grid area poles; AB – Arkona Basin, BB – Bornholm Basin, BS – Bothnian Sea, and BoB – Bothnian Bay

At solid boundaries, the following conditions were prescribed: zero heat and salt fluxes; hydrodynamic conditions of no-slip and free slip for current velocities.

Model calculations were carried out for the period from January 1, 2014, to December 31, 2015, with hourly averaged output.

Numerical experiment on modeling free oscillations in the North and Baltic Seas system. Such modeling was carried out using the three-dimensional baroclinic INMOM model described above. Initially, to bring the water masses out of equilibrium, real wind and atmospheric pressure fields from the ERA5 reanalysis were prescribed as boundary conditions at the sea surface for one week. Then all external forcing was switched off, the coefficients of vertical turbulent viscosity, diffusion, and bottom friction were set to zero, and the coefficients of horizontal turbulent viscosity and diffusion were set to the minimum possible level. The liquid boundaries in the North Sea were replaced by solid ones. This condition has drawbacks associated with the fact that long gravity waves reflect from the solid boundary and, interacting with incoming waves, form standing modes of wave motion. This can lead to the formation of amphidromic systems and antinodes in sea level fields that are not observed in reality. In a number of studies of free oscillations using numerical experiments, a radiation condition is prescribed at the liquid boundary, which simulates the continuation of the marine basin beyond it [35, 36]. However, this condition works well only for long waves incident normally (perpendicularly) to the

boundary and propagating at a constant depth. With oblique incidence of long waves on the liquid boundary or complex bottom topography, their reflection also occurs [35].

We carried out free oscillation modeling for the period from January 8 to December 8, 2014, with a time step of 10 s. Calculation results were saved every hour.

The amplitude-phase characteristics of free sea level oscillations were estimated using the fast Fourier transform at each point of the field:

$$f(t) = Z_0 + \sum_{k=1}^{N/2}(a_k \cos k\,\omega t + b_k \sin k\,\omega t), \quad \left(\omega = \frac{2\pi}{T}, k = 0, 1, 2, \ldots\right), \qquad (1)$$

where $f(t)$ is the original sea level time series; N is the series length; T is the period; t is time; a_k and b_k are expansion coefficients corresponding to their frequency ω; Z_0 is the mean value of the series; k is the coefficient number.

Amplitude (A_k) and phase (F_k) were calculated as follows:

$$A_k = \sqrt{a_k^2 + b_k^2}, \quad F_k = \arctan\left(\frac{b_k}{a_k}\right). \qquad (2)$$

Based on the Fourier analysis, amplitude spectra of the simulated sea level oscillations were constructed, which made it possible to assess the frequency recurrence of amplitude maxima.

For frequencies corresponding to the identified amplitude maxima, the propagation velocities of sea level oscillations were calculated from phase shifts between grid nodes:

$$C_x = \frac{\Delta x \cdot 360}{T\Delta F_x}, C_y = \frac{\Delta y \cdot 360}{T\Delta F_y}, C_{Sa} = \sqrt{C_x^2 + C_y^2}, \qquad (3)$$

where C_x, C_y are the velocity components along the parallel and meridian; Δx, Δy are distances between adjacent grid nodes; C_{Sa} is the velocity magnitude; T is the oscillation period; ΔF_x, ΔF_y are phase difference components between grid nodes.

Methods for analyzing the spatiotemporal variability of hydrometeorological information.

Decomposition of oceanological and meteorological fields into complex empirical orthogonal functions (CEOF). To analyze the spatiotemporal variability of hydrometeorological fields, the CEOF method was applied. Unlike the traditional EOF method, which is limited to describing standing oscillations and does not account for the spatial movement of wave structures, the CEOF method is based on the use of complex quantities and singular value decomposition. This approach makes it possible to identify propagating wave signals [37].

The CEOF method allows a comprehensive study of the spatiotemporal variability of fields, identifying the dominant spatial modes of variability, their temporal dynamics, and quantifying the contribution of each mode to the total variance of the process under study [37].

Cross-correlation analysis of vector processes. To analyze the mechanisms of generation of synoptic current oscillations under the influence of anemobaric factors, a cross-correlation analysis of current perturbations $\mathbf{V}(t)$ and tangential wind stress $\boldsymbol{\tau}(t)$ was performed, following the methodology developed in studies [5] [38]. The tangential wind stress was estimated according to the following formula:

$$\boldsymbol{\tau} = c\rho_a \mathbf{W}|\mathbf{W}|, \tag{4}$$

where ρ_a = 1.2754 (kg/m^3) is air density; c = 0.0012 ($|\mathbf{W}|$ 0.066 + 0.63) is the air-sea friction coefficient; $\mathbf{W}$ is the wind velocity vector from the ERA5 reanalysis. Cross-correlation analysis was performed by calculating two invariants of the cross-correlation tensor function $K_{\mathbf{VU}}(\theta)$:

$$K_{\mathbf{VU}}(\theta) = \begin{pmatrix} K_{V_1U_1}(\theta), & K_{V_1U_2}(\theta) \\ K_{V_2U_1}(\theta), & K_{V_2U_2}(\theta) \end{pmatrix}, \tag{5}$$

where $\mathbf{V}(t)$ and $\mathbf{U}(t)$ are vector processes (current and tangential wind stress); V_1, V_2 are the components of vector process $\mathbf{V}(t)$ along the parallel and meridian, respectively; U_1, U_2 are components of vector process $\mathbf{U}(t)$ along the parallel and meridian, respectively; t is time; θ is the time lag.

Linear invariant $I_1^{\mathbf{VU}}(\theta)$ equals the trace of the correlation tensor function matrix (5) and characterizes the commonality of intensities of collinear changes in the vector processes $\mathbf{V}(t)$ and $\mathbf{U}(t)$.

The rotation indicator $\Omega^{\mathbf{VU}}(\theta)$ equals the difference of the off-diagonal components of the correlation tensor function matrix (5) and characterizes the commonality of orthogonal changes in the processes $\mathbf{V}(t)$ and $\mathbf{U}(t)$. If $\Omega^{\mathbf{VU}}(\theta) > 0$, then the process $\mathbf{U}(t)$ is, on average, rotated clockwise relative to the process $\mathbf{V}(t)$ over a given time interval; if $\Omega^{\mathbf{VU}}(\theta) < 0$, it is rotated counterclockwise.

After normalizing $I_1^{\mathbf{VU}}(\theta)$ and $\Omega^{\mathbf{VU}}(\theta)$ by the linear invariant of the variance tensor, according to [35], their normalized values $r_{I_1}^{\mathbf{VU}}(\theta)$ and $r_{\Omega_1}^{\mathbf{VU}}(\theta)$ were calculated.

Then the total correlation coefficient was calculated:

$$R_{\mathbf{VU}}(\theta) = \sqrt{\left[r_{I_1}^{\boldsymbol{VU}}(\theta)\right]^2 + [r_{\Omega_1}^{\boldsymbol{VU}}(\theta)]^2}. \tag{6}$$

Spectral analysis of current oscillations. To calculate the spectral structure of synoptic-scale current oscillations, two invariants of the spectral tensor function $S_{\mathbf{V}}(\omega)$ were estimated:

$$S_{\mathbf{V}}(\omega) = \begin{pmatrix} S(\omega)_{uu}, & S(\omega)_{uv} \\ S(\omega)_{vu}, & S(\omega)_{vv} \end{pmatrix}. \tag{7}$$

The linear invariant $I_1(\omega)$ of the spectral density tensor equals the trace of the spectral tensor function matrix $S_{\mathbf{V}}(\omega)$ and, according to [6], characterizes

[5] Belyshev, A.P., Klevantsov, Yu.P. and Rozhkov, V.A., 1983. *Probability Analysis of Sea Currents*. Leningrad: Gidrometeoizdat, 264 p. (in Russian).

[6] Rozhkov, V.A., ed., 1984. *Methodological Letter on Probability Analysis of Vector Time Series of Current and Wind Speeds*. Leningrad: Gidrometeoizdat, 61 p. (in Russian).

the frequency distribution of the intensity modulus of oscillations of collinear current velocity components in any direction.

The linear invariant $I_1(\omega)$ of the spectral tensor, calculated as the trace of the matrix of the spectral tensor function $\mathbf{S_v}(\omega)$, quantitatively characterizes the frequency distribution of the intensity of collinear flow velocity fluctuations regardless of their spatial orientation. According to [6], this invariant represents a measure of the intensity of current fluctuations in all directions, which makes it possible to analyze the overall dynamics of perturbations without considering their vector structure.

The invariant $\Omega(\omega)$ of the spectral tensor $S_{\mathbf{v}}(\omega)$, defined through the difference of its off-diagonal components (formula (7)), quantitatively describes the frequency distribution of the energy of orthogonal oscillations of current velocities. This parameter serves as an indicator of the rotational component of current dynamics: its magnitude reflects the intensity of velocity vector rotation at a given frequency, and its sign indicates the prevailing direction of rotation – positive values correspond to cyclonic (clockwise) rotation, and negative values correspond to anticyclonic (counterclockwise) rotation.

Cross-spectral analysis of wind and current oscillations. To study the frequency characteristics of the relationship between synchronous time series of current oscillations and tangential wind stress at each point of the computational domain, cross-spectral analysis was applied. The cross-spectral density function $S_{\mathbf{VU}}(\omega)$ between two vector processes $\mathbf{V}(t)$ and $\mathbf{U}(t)$ was defined as the Fourier transform of the tensor function $K_{\mathbf{VU}}(\theta)$:

$$S_{\mathbf{VU}}(\omega) = \frac{1}{2\pi}\int_{-\infty}^{\infty} \mathrm{e}^{-i\omega t} K_{\mathbf{VU}}(\theta)dt. \qquad (8)$$

According to the methodology described in [5, 6], the following invariants were calculated: $|I_1^{\mathbf{VU}}(\omega)|$, $\psi(\omega)$, $|\Omega^{\mathbf{VU}}(\omega)|$, $f(\omega)$, $F^2_{\mathrm{col}}(\omega)$, and $F^2_{\mathrm{orth}}(\omega)$. The invariant $I_1^{\mathbf{VU}}(\omega)|$ characterizes the commonality modulus of intensities of collinear changes of the vector processes $\mathbf{V}(t)$ and $\mathbf{U}(t)$ in the frequency domain; the invariant $\psi(\omega)$ characterizes the phase lag of the corresponding harmonics of time series $\mathbf{V}(t)$ and $\mathbf{U}(t)$ relative to each other. The invariant $|\Omega^{\mathbf{VU}}(\omega)|$ characterizes the commonality modulus of the intensities of orthogonal changes of the vector processes $\mathbf{V}(t)$ and $\mathbf{U}(t)$ in the frequency domain; the invariant $f(\omega)$ characterizes the phase lag of corresponding harmonics of time series $\mathbf{V}(t)$ and $\mathbf{U}(t)$ relative to each other.

Invariants $F^2_{\mathrm{col}}(\omega)$ and $F^2_{\mathrm{orth}}(\omega)$ of the coherence tensor quantitatively characterize the degree of synchronization of two vector processes in the frequency domain. The first invariant ($F^2_{\mathrm{col}}(\omega)$) reflects the measure of consistency of collinear oscillation components, showing how synchronously the unidirectional vector components change. The second invariant ($F^2_{\mathrm{orth}}(\omega)$) estimates the coherence of orthogonal components, revealing the relationship between perpendicular components of the processes.

Results

Decomposition of hydrometeorological fields into CEOF. According to the results presented in Table 1, for the North and Baltic Seas area during the autumn-winter period of 2014 (November–December), it was found that the first five CEOFs describe 97% of the total variance of sea level oscillations. There is a pronounced dominance of the first mode (77% of the variance). The second mode describes 10% of the variance, the third mode 6%, and the fourth and fifth modes together account for less than 4% of the variance. In the variability of atmospheric fields, the first CEOF impact, although dominant, is significantly smaller compared to that on sea level, amounting to 33–53%. For atmospheric processes, there is also an increase in the contribution of other CEOFs to the variance.

Table 1

Comparative contributions (%) of the first five CEOFs to the total dispersion of hydrometeorological fields in the North and Baltic Seas region for November 1 – December 31, 2014

Characteristic	CEOF				
	first	second	third	fourth	fifth
Sea level (INMOM)	77	10	6	3	1
Atmospheric pressure	53	27	10	5	2
Tangential wind stress $\boldsymbol{\tau}$	33	17	12	8	7

Fig. 2 shows the first three CEOF decomposition modes of sea level fields in the North and Baltic Seas, obtained using the baroclinic INMOM model during MBI development in autumn–winter 2014. Analysis of the amplitude distribution revealed regional features: in the North Sea, the maximum values of the first and second modes are concentrated in the southeastern part (Fig. 2, *a*, *c*), whereas the third mode exhibits the greatest intensity in the southwest (Fig. 2, *e*). In the Baltic Sea, the spatial pattern is different – the first mode reaches a maximum in the Gulf of Riga (Fig. 2, *a*), and the second and third modes show the greatest amplitudes in the southwestern area (Fig. 2, *c*, *e*).

Spatial distributions of phase estimates indicate significant heterogeneity of phase changes: in some rather large sea areas, a relatively monotonic phase change is observed; in others, small in space, it changes very sharply, by 180° (Fig. 2, *b*, *d*, *f*). The monotonic nature of phase changes of the first and third CEOFs indicates predominant propagation of sea level inhomogeneities in the North Sea from west to east, and in the Baltic Sea for these modes from northeast to southwest, whereas for the second CEOF in the Baltic Sea, the opposite direction of disturbance propagation is observed – from southwest to northeast. In the north and south of the North Sea, as well as in the Norwegian Trench, all three CEOFs show degenerate amphidromic systems and nodal zones where sea level oscillations are zero and the phase changes by 180° (Fig. 2, *right*). The presence of degenerate amphidromy in the second mode at the entrance to the Skagerrak Strait leads to the formation of anticyclonic movement of sea level disturbances in the North Sea (Fig. 2, *d*). For the third CEOF, nodal zones are also observed in the Baltic Sea at the entrance to the Gulfs of Finland

and Riga, as well as in the center of the Bothnian Bay (Fig. 2, *e*, *f*). In the north of the Danish Straits and the Kattegat Strait, sea level oscillations for all three CEOFs have low values and sharp phase changes close to 180°, which may indicate dynamic conditions close to a nodal zone in standing oscillations. The described results indicate that the response of sea level fields in the North and Baltic Seas system to the impact of anemobaric forces during MBIs occurs in the form of low-frequency wave processes demonstrating characteristics of both progressive and standing waves.

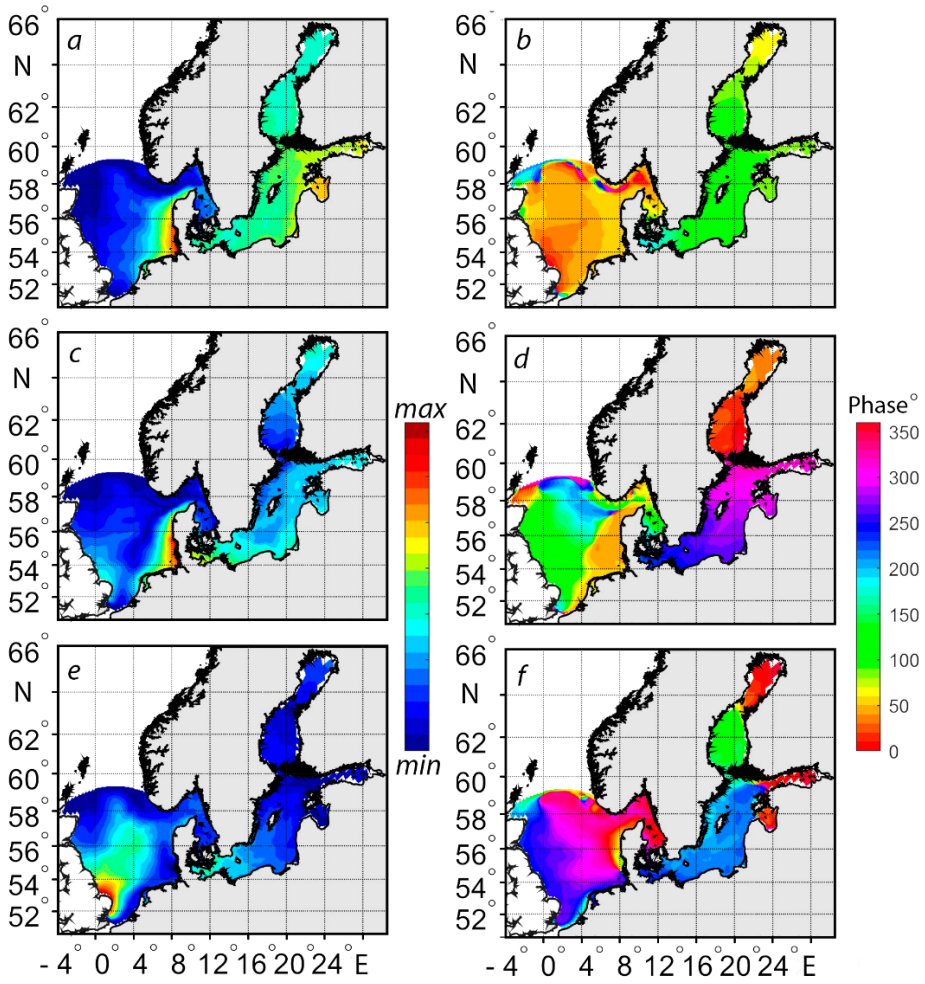

F i g. 2. Spatial distribution of amplitudes (*left*) and phases (*right*) of the first three CEOFs in the sea level field of the North and Baltic Seas in November–December 2014, based on the results of numerical simulation using the INMOM model: *a*, *b* – the first CEOF; *c*, *d* – the second CEOF, and *e*, *f* – the third CEOF

Cross-correlation analysis of the principal decomposition components of the sea level and atmospheric process fields into CEOFs, the results of which are given in Table 2, provides insight into the degree of relationship between the variability of these fields over the entire area of the two seas. It indicates that a high correlation (0.67) is observed only between the first principal components of sea level and

atmospheric pressure. Between all principal components of wind field variability and sea level, the correlation is low.

Results of cross-wavelet analysis of the first principal components of decomposition into CEOFs of sea level and atmospheric pressure fields in the region under study indicate that in November–December 2006, when there was no MBI, the relationship between the variability of sea level and atmospheric pressure fields occurred at periods of about 2–4 days, where it was close to inverse, and coherence values at certain time intervals were high, 0.6–0.95 (Fig. 3, *a*). Such periods of variability of atmospheric pressure and sea level fields are associated with the passage of cyclones [39]. In the lower frequency range, there was no relationship between the variability of sea level and atmospheric pressure fields. During the formation and propagation of the MBI in November–December 2014, the structure of the relationship between the first principal components of decomposition of sea level and atmospheric pressure fields into CEOFs changes significantly: the main energy transfer between the variability of baric fields and sea level occurs in a lower frequency range at periods of 6–22 days, where coherence values varied within the range of 0.65–0.95.

Table 2

Correlation coefficients between the principal components of atmospheric characteristic fields and sea level decomposed into CEOF

Characteristic	Sea level				
	first CEOF	second CEOF	third CEOF	fourth CEOF	fifth CEOF
Atmospheric pressure	+0.67	+0.25	–0.12	+0.02	+0.36
Zonal component τ_x	–0.51	+0.03	+0.17	–0.10	+0.37
Meridional component τ_y	+0.19	–0.30	+0.12	+0.29	+0.10

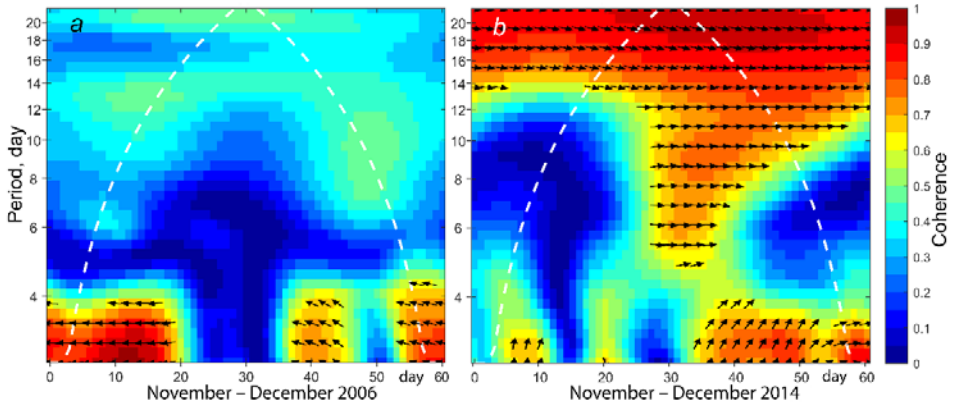

Fig. 3. Results of cross-wavelet analysis of the first principal components of sea level and atmospheric pressure fields decomposed into CEOFs in the North and Baltic Seas system for November–December, 2006 (*a*) and 2014 (*b*). The arrow directed eastward means that the phase difference between the processes is 0°; the one directed westward indicates 180°; arrows with a northward component indicate that sea level disturbances described by the first CEOF are ahead of similar disturbances in the atmospheric pressure field. Phase estimates are given only for coherence values ≥ 0.6. White dashed lines indicate the confidence interval of the wavelet analysis estimates

Results of cross-correlation analysis of tangential wind stress and current oscillations. Analysis of spatial features of the relationship between the variability of **τ** and **V** from the GLORYS reanalysis during MBI formation was carried out by calculating the maximum correlation coefficients $R_{\mathbf{VU}}(\theta)$ (formula (6)) at the corresponding time lags (θ) at each point of the computational domain (Fig. 4). For comparison, the same estimates were made for November–December 2006, when no MBI was recorded [14].

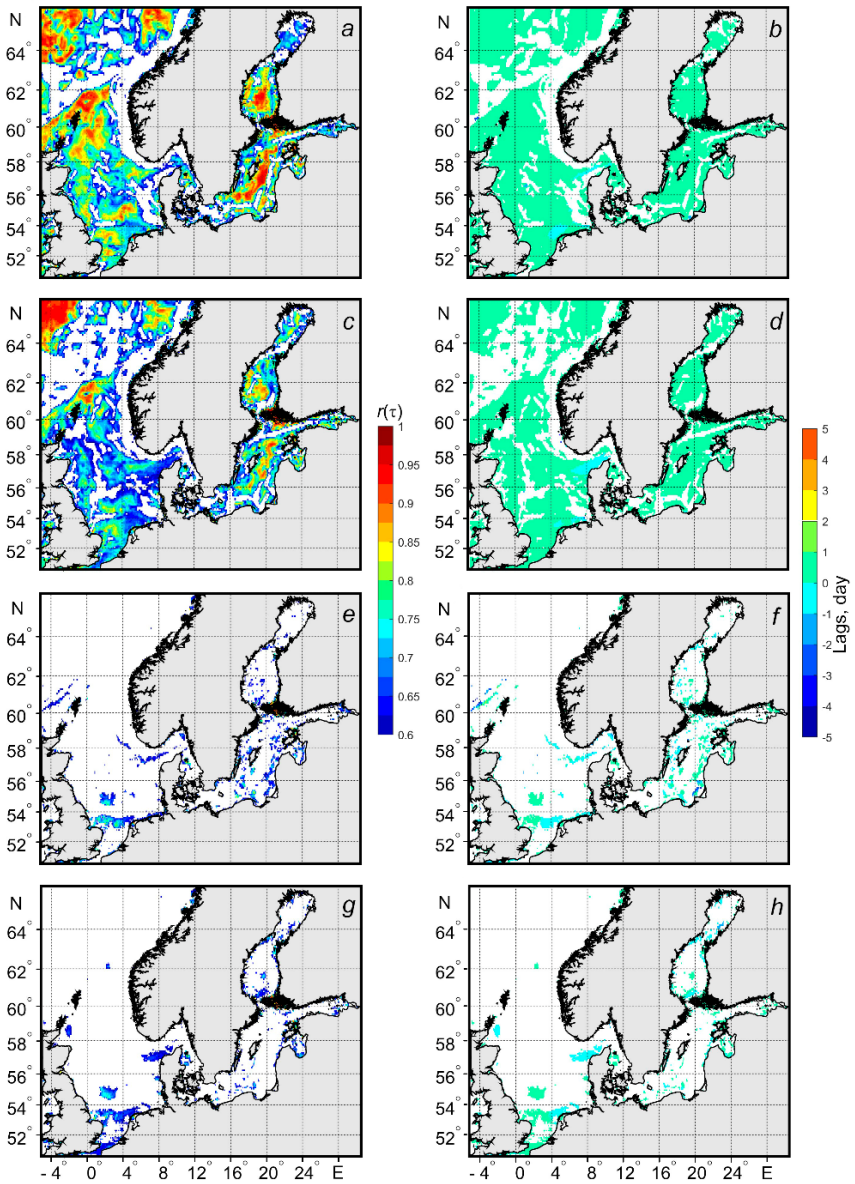

F i g. 4. Maximum correlation coefficients (*left*) and time lags (*right*) between tangential wind stress oscillations and surface (*a* – *d*) and bottom (*e* – *h*) currents in November–December 2014 (*a*, *b*, *e*, *f*) and 2006 (*c*, *d*, *g*, *h*), calculated using GLORIS. Correlation coefficient values are ≥ 0.6

High values of synchronous coupling between **τ** and surface **V**, reaching 0.60–0.95, are observed in most areas of the North and Baltic Seas, except for the Norwegian Trench, certain areas of the central and southeastern sectors of the North Sea, the Skagerrak and Kattegat Straits, as well as narrow coastal zones of the southern, eastern, and northern Baltic, the Gulf of Finland, and the northern part of the Gulf of Bothnia (Fig. 4, *a*, *c*).

Comparative analysis showed significant differences between 2014 and 2006: during the period without an MBI (2006), a decrease in correlation was observed, and zones where a statistically significant relationship between wind and surface currents was absent expanded (Fig. 4, *c*, *d*).

In the bottom layer, the relationship between **τ** and **V** is absent in most sea areas. Exceptions include some relatively shallow areas with depths of 15–40 m, where correlation coefficients between **τ** and bottom **V** reach 0.60–0.70 (Fig. 4, *e* –*h*).

Spectral analysis of current oscillations. Analysis of the spectra of current oscillations in the southwestern Skagerrak Strait during the formation and propagation of the MBI, calculated from GLORYS reanalysis data and the results of the numerical experiment with the INMOM model, revealed the following features in the spectral density estimates. The values of the linear invariant $I_1(\omega)$ at energy-carrying frequencies exceed those of the rotation indicator $\Omega(\omega)$ by several times, and in some cases by an order of magnitude, indicating a predominance of collinear changes in current velocities over their orthogonal oscillations during the formation of synoptic current variability.

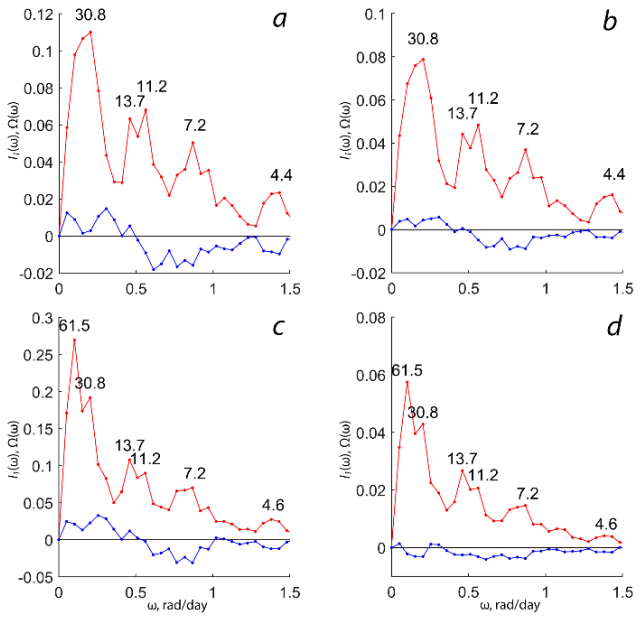

F i g. 5. Linear invariant $I_1(\omega)$ (red line) and rotation indicator $\Omega(\omega)$ (blue line) of the spectral tensor function of current oscillations in the surface (*left*) and bottom (*right*) layers in the southwestern Skagerrak Strait, based on GLORIS reanalysis data (*a*, *b*) and the results of the numerical experiment using the INMOM model (*c*, *d*). Numbers on the peaks are the periods of the spectrum peaks (days)

Analysis of rotational characteristics showed that for periods of 31–61 days, cyclonic rotation of velocity vectors prevails ($\Omega(\omega) > 0$), whereas at shorter periods, anticyclonic rotation is observed ($\Omega(\omega) < 0$) (Fig. 5). Spectral maxima in both the surface and bottom layers have the highest values in the low-frequency range (31–62 days), while less intense peaks correspond to periods of 11–14, 7, and 4 days (Fig. 5).

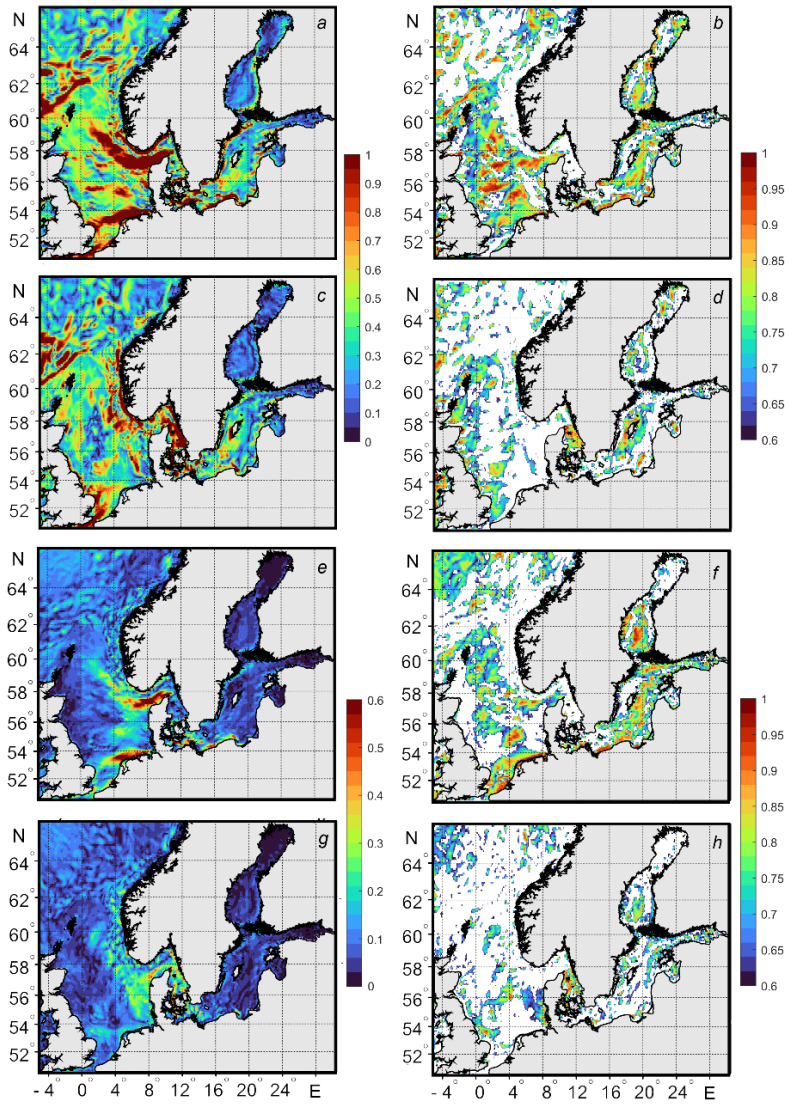

F i g. 6. Estimates of cross-spectral density (*left*) and coherence (*right*). Left – invariants $|I_1^{VU}(\omega)|$ (*a*, *e*) and $|\Omega^{VU}(\omega)|$ (*c*, *g*) of the cross-spectral density tensor, right – invariants $F^2_{col}(\omega)$ (*b*, *f*) and $F^2_{orth}(\omega)$ (*d*, *h*) of the coherence tensor between synoptic-scale surface current oscillations and tangential wind stress for periods of 30.5 (*a* – *d*) and 12.2 (*e* – *h*) days. Regions with coherence values ≥ 0.6 are shown

Cross-spectral analysis of tangential wind stress and current oscillations. Figs. 6 and 7 show, for three frequencies of energy-carrying maxima identified in

the current oscillation spectra (Fig. 5), the spatial distributions of estimates of two invariants of the cross-spectral density tensor $|I_1^{\mathbf{VU}}(\omega)|$, $|\Omega^{\mathbf{VU}}(\omega)|$ and two invariants of the coherence tensor $F^2_{\text{col}}(\omega)$, $F^2_{\text{orth}}(\omega)$ between $\boldsymbol{\tau}$ and $\mathbf{V}$ during MBI formation and propagation. Common to all these cases is that the maximum values of the invariants $|I_1^{\mathbf{VU}}(\omega)|$, $|\Omega^{\mathbf{VU}}(\omega)|$, which correspond to high coherence values, are not observed everywhere, but only in relatively localized zones of the seas. Such zones in the North Sea are the Skagerrak Strait, certain areas of the Norwegian Trench, the shallow southeastern and southern parts of the sea, and, for variability periods of about a month, some areas of the northwestern and central parts of the sea. In the Baltic Sea, similar areas are observed in the Kattegat Strait, the coastal zone of the southern part of the sea, areas of the central Baltic around Gotland Island, localized areas in the Gulf of Riga, a narrow coastal zone in the east of the Bothnian Sea, and some local areas of its central part.

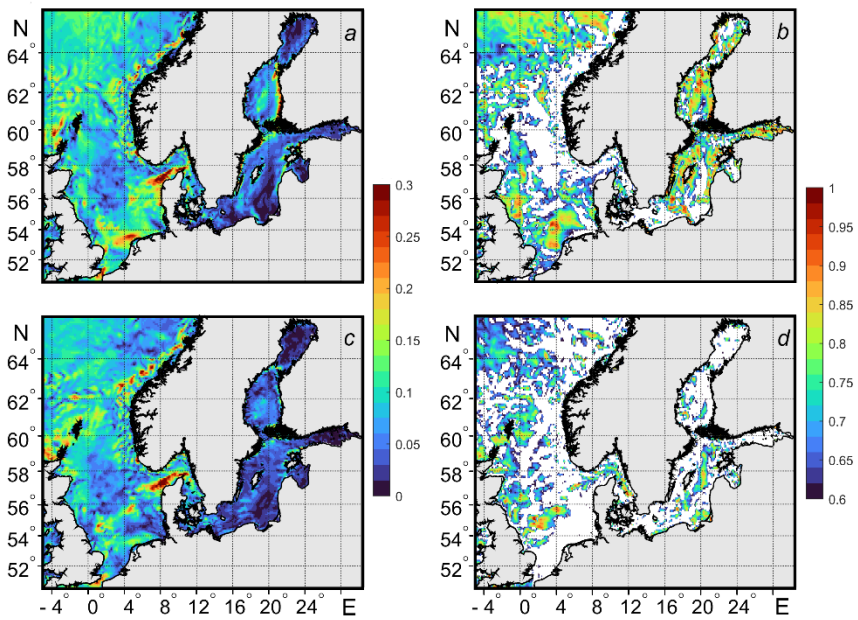

F i g. 7. Same as in Fig. 6. Left – invariants $|I_1^{\text{VU}}(\omega)|$ (*a*) and $|\Omega^{\text{VU}}(\omega)|$ (*c*), right – invariants $F^2_{\text{col}}(\omega)$ (*b*) and $F^2_{\text{orth}}(\omega)$ (*d*) for a 7-day period. Regions with coherence values ≥ 0.6 are shown

It is important to note that areas with high values of cross-spectral density and coherence between $\boldsymbol{\tau}$ and $\mathbf{V}$ in the North Sea are located in frontal zones separating the lower-salinity waters propagating along the Norwegian Trench from the Baltic, as well as waters freshened by river runoff from the southern and southeastern coasts, from the saline waters of the central North Sea.

Spectral structure and propagation velocities of free sea level disturbances in the North and Baltic Seas system. Analysis of free oscillations of the sea surface is an important task in physical oceanography because it allows us to understand the nature of natural oscillations of marine basins. Natural oscillations can be considered as potential capabilities of a dynamic system, the spectral properties of

which depend on the morphometric characteristics of the water area – its size, bathymetry, and coastline configuration. As studies show [39, 40], the relaxation of water masses to a state of rest after the cessation of external forcing usually occurs at the characteristic frequencies of natural oscillations. Of particular importance is the resonance mechanism, in which the frequency of natural oscillations of a marine basin becomes equal to the frequency of anemobaric disturbances, leading to the generation of anomalously large inhomogeneities in the fields of oceanographic parameters [41–43].

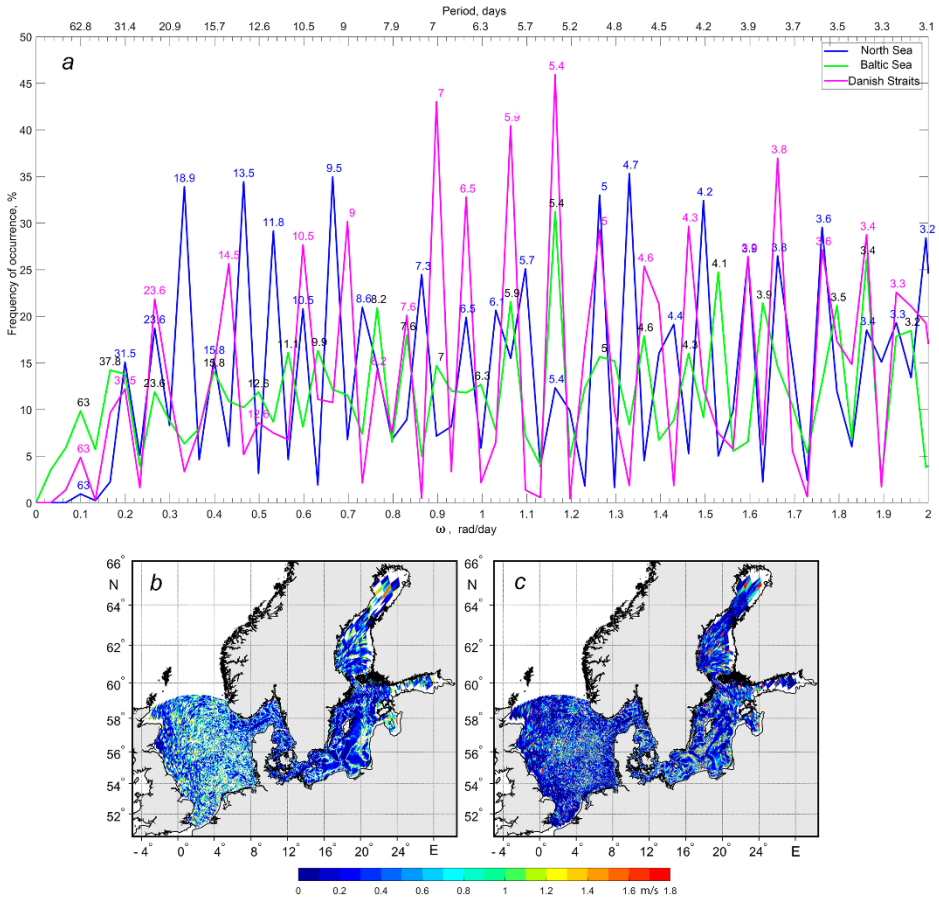

F i g. 8. Recurrence (%) of amplitude maxima in the Fourier spectra of free sea level oscillations in the North and Baltic Seas system based on numerical experiments using the INMOM model (*a*), as well as phase velocities of free waves in the sea level field with periods of 62 (*b*) and 32 (*c*) days

The numerical experiment described above with the three-dimensional baroclinic INMOM model, aimed at obtaining information on the characteristics of natural oscillations in the stratified environment of the North and Baltic Seas, showed that in the synoptic range of time scales, the Fourier amplitude spectra of free sea level oscillations in different sea areas have a multi-peak structure. Fig. 8, *a* presents generalized information on the spectral structure of natural oscillations in the North and Baltic Seas system. In the North Sea, amplitude maxima were most

often recorded at periods of 18.9, 13.5, 9.5, 5.0, 4.7, 4.2, and 3.6 days, with recurrence reaching 30–35%. The highest recurrence (40–47%) was observed for free sea level oscillations with periods of 7, 5.9, and 5.4 days in the Kattegat and Danish Straits. In the Baltic Sea, the recurrence of free oscillation peaks in the vast majority of cases is below 25%. Exceptions are the Baltic natural oscillations with a period of 5.4 days, whose recurrence is 33%, and those with a period of 3.4 days, with a recurrence of 27%. It is also important to note that the frequencies of the main energy-carrying maxima in the current oscillation spectra during the formation and propagation of the MBI (Fig. 5) are close to the frequencies of natural oscillations in the North and Baltic Seas system (Fig. 8, *a*). The phase velocities of free waves in the sea level field, calculated using formulas (3), vary in the range of 0.2–1.8 m/s. These values are significantly lower than theoretical estimates for barotropic gravity waves given by the relation $C = \sqrt{gH}$ (C is the phase velocity, g is the acceleration due to gravity, and H is the sea depth), which yields characteristic speeds of about 30.5 m/s for the North Sea (with an average depth of 95 m) and 23 m/s for the Baltic (with a depth of 54 m). However, the observed velocities agree well with the theoretical dispersion relations of baroclinic modes of topographic waves and Kelvin waves [6, 18, 40].

Discussion of results

Major inflows are excited by forces of the horizontal atmospheric pressure gradient (**grad**P_a) and, to a greater extent, by tangential wind stress in atmospheric cyclones and anticyclones moving over the North Atlantic and Europe [2, 4–7, 9, 15]. However, the response of water masses to the impact of $\boldsymbol{\tau}$ can be different. It can be local, when at each point of the sea, under the action of tangential wind stress combined with the Earth's rotation, wind-driven currents and associated setup/setdown sea level oscillations are excited (Ekman mechanism) [7] [44]. However, this response can also be wave-like, when large-scale low-frequency waves, similar to Rossby and Kelvin waves, are generated under the action of disturbing forces [45, 46]. A sign of wave motion is a monotonic change in the phase of sea level oscillations at frequencies of significant energy-carrying maxima, indicating the spatial propagation of the waveform.

Low-frequency waves can be generated by the direct action of anemobaric forces or as a result of resonance of these forces with the natural oscillations of marine basins. Under conditions of significant confinement of marine basins, progressive waves are modified into progressive-standing modes of low-frequency waves [33], characteristic of closed basins. Signs of such modes are the presence of nodes, nodal lines (where sea level oscillations are zero and horizontal current components are maximal), and antinodes with maximum amplitudes of sea level oscillations. Between nodal lines in such a wave field, a quasi-monotonic change in wave phase is observed. A theoretical description of these waves and the kinematics of their motions is presented in [22, 23, 47]. It is precisely such features of

[7] German, V.Kh. and Levikov, S.P., 1988. [*Probabilistic Analysis and Modeling of the Sea Level Oscillations*]. Leningrad: Gidrometeoizdat, 231 p. (in Russian).

spatiotemporal variability of the sea level fields of the North and Baltic Seas that are observed from the results of their decomposition into CEOFs (Fig. 2), which indicates a predominantly wave-like response of the water masses to the forcing of anemobaric forces during the formation and propagation of the 2014 MBI. Due to the significant confinement of the North and especially the Baltic Sea, the response of water masses to external disturbing forces occurs in the form of progressive-standing modes of gradient-vortex waves. Similar features of the amplitude-phase characteristics of low-frequency sea level oscillations in the Baltic and North Seas system during the MBIs of 1993 and 2003 were also noted in [7, 40] based on the analysis of altimetric information and were explained by a mode of topographic Rossby waves characteristic of closed basins.

At the same time, studies of vertical current profiles from regional reanalysis of hydrophysical fields and results of the numerical experiment with the three-dimensional baroclinic hydrodynamic model INMOM did not reveal the presence of an Ekman spiral in the vertical structure of current vectors during MBIs [7, 40]. The results of cross-correlation and cross-spectral analysis presented in Figs. 4 and 6 demonstrate extensive areas where there is no relationship between oscillations of tangential wind stress and currents during MBIs. These results indicate that, due to the large spatiotemporal variability of wind and the baroclinicity of water masses, stable and intense drift currents do not have time to form, and the response of water masses to the impact of anemobaric forces during MBIs is largely wave-like.

Due to the significant polycyclicity of atmospheric pressure and wind variability, the dynamic response of water masses to atmospheric processes occurs in different frequency ranges. Our spectral analysis of current oscillations during MBIs demonstrates the presence of spectral density peaks at periods of about 4, 7–14, and 31–61 days (Fig. 5). Current oscillations with a period of 4 days can be caused by the movement of atmospheric cyclones and anticyclones, whose average transit period over northwestern Europe, according to [44, 48], is close to 1–3 days. Oscillations with periods of 7–14 days are associated with the natural synoptic period, which according to some sources is 5–8 days [48], and according to others reaches 15 days [7]. In [38], the authors associate oscillations with periods from several weeks to months in the North Atlantic with global changes in atmospheric circulation, where variations in the zonal circulation index play a significant role. In [6], it was shown that during the MBIs of 1993 and 2003, sea level disturbances with characteristic periods of 1–2 months in the North and Baltic Seas system are identified as baroclinic Rossby waves having wavelengths in the range of 200–1600 km and phase velocities in the range of 0.04–0.35 m/s.

Analysis of various hydrometeorological information indicates that in November–December 2006, when no MBI was observed, energy transfer from baric fields to water mass movements in the North and Baltic Seas system occurred in the period range of several days (Fig. 3), corresponding to the time scales of moving atmospheric cyclones and anticyclones [44, 48]. During the formation and propagation of the MBI in November–December 2014, the main energy transfer from baric fields occurred in the period range of several weeks (Fig. 3). Results of spectral analysis of current oscillations at the entrance to the Skagerrak Strait show

that in the autumn-winter season of 2014, the highest spectral density peaks were recorded not in the range of characteristic periods of atmospheric cyclones/anticyclones and the natural synoptic period, but in a significantly lower frequency range of 31–62 days (Fig. 5). These periods agree with the periods of natural oscillations in the North and Baltic Seas system estimated in this work using a numerical experiment with the three-dimensional baroclinic hydrodynamic model INMOM (Fig. 8, *a*).

In [18], using regional reanalysis of hydrophysical fields, the temporal changes in vertical profiles of current velocity in the north of the Danish Straits during the formation and propagation of the 2014 MBI were studied. It was demonstrated that in November 2014, for 25 days, currents in the Øresund and Great Belt Straits were directed from the Baltic to the Kattegat Strait, and in December, for 22 days, conversely, from the Kattegat to the Baltic; then their direction changed again to the opposite. The average daily current velocities reached very high values of 1.2–1.4 m/s [18]. At this time, the level in the eastern North Sea oscillated with the greatest amplitude in antiphase with the level in the southwestern Baltic (Fig. 2, *a–d*), creating large level gradients between the North and Baltic Seas, reaching 1 m [16]. These results indicate that in the North Sea–Danish Straits–Baltic system during the autumn-winter period of 2014, under the influence of some uncharacteristic meteorological conditions, a non-stationary low-frequency wave process with a pronounced standing component (which had one of the nodal zones in the Danish Straits area) formed in the water mass movements, a fragment of which was the MBI.

Analysis of the synoptic situation over the North Atlantic and Europe during the autumn-winter period of 2014 reveals that in November, the dynamic regime of the Baltic and North Seas was formed under the influence of a stable anticyclone that occupied a vast area from the Norwegian Sea to the Black Sea (Fig. 9, *a*). The anticyclone created a powerful blocking effect, hindering the normal movement of Atlantic cyclones in the northeast direction, which significantly altered the nature of wind forcing and circulation processes in the region. This led to the fact that for more than three weeks, winds of easterly directions blew over the Baltic and North Seas [5], which caused an outflow of water from the Baltic, which, together with the static effect of atmospheric pressure, caused a decrease in its sea level. In early December 2014, the synoptic situation changed: the anticyclone began to break down, shifting southeast, and deep atmospheric cyclones began to move freely from the North Atlantic to the Barents Sea region (Fig. 8, *b*); as a result, intense westerly and southwesterly winds blew over the North and Baltic Seas, causing a significant setup of level in the North Sea. For this reason, the North Sea level began to rise relative to the Baltic level, leading to the start of the MBI. But such synoptic situations in the North Atlantic – Western Europe region occur frequently in the autumn-winter period [4, 7, 14, 47], while MBIs are very rare events, occurring once every 10–11 years in recent decades [4, 6, 7, 9, 15, 16].

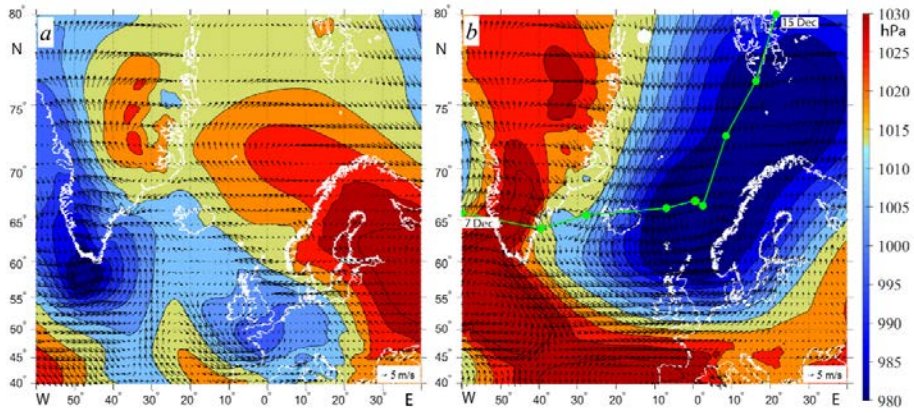

F i g. 9. Atmospheric pressure and wind fields over the North Atlantic and Western Europe on November 16 (*a*) and December 11 (*b*), 2014, based on the ERA5 atmospheric field reanalysis data. The green broken line with dots shows the cyclone trajectory from December 7 to December 15, 2014. Points are plotted at 1-day intervals

It should be noted that on December 11, a sharp slowdown of the deep cyclone occurred, from an initial speed of 7–11 m/s to 1.0 m/s (Fig. 9, *b*). It was on this day that the difference in the average daily sea level between the Kattegat Strait and the southwestern Baltic reached its maximum values during the MBI period, up to 1 m [18]. This decrease in cyclone speed made it comparable to the phase velocities of free low-frequency waves with periods of 32–62 days in the North and Baltic Seas (Fig. 8, *b*, *c*), creating conditions under which resonance could occur between the anemobaric forces in the cyclone and the natural oscillations of the marine basin. A similar slowdown of baric formations in the eastern North Atlantic was observed during MBI formation in 1993 and 2003 [17]. The possibility of resonance is also indicated by the high coherence values between changes in atmospheric pressure and sea level (Fig. 3), as well as $\boldsymbol{\tau}$ and **V** (Fig. 7) at zero lags at the frequencies of the identified energy-carrying cross-spectrum maxima. As a result of such resonance, a high-amplitude forced progressive-standing low-frequency wave could be generated with a nodal zone in the area of the Kattegat Strait and Danish Straits (Fig. 2), which strongly "rocked" the water masses of the North and Baltic Seas, leading to a significant level difference between them and a sharp increase in current velocities in the strait zone between the two seas to 1.2–1.4 m/s [18, 45], affecting the MBI intensity. After December 12, the cyclone's direction changed to north-northeast, its speed increased again to 7 m/s (Fig. 9, *b*), and the level gradient between the Kattegat Strait and the southwestern Baltic began to decrease [18].

The results we obtained are insufficient to confirm the resonance hypothesis. It is necessary to conduct additional numerical experiments in which the computational domain of our model should be expanded to include the North Atlantic; wind and atmospheric pressure fields in a simulated cyclone moving along a trajectory characteristic of the 2014 MBI should be prescribed as boundary conditions at the sea surface, as was done, for example, in [43, 46]; then a series of numerical experiments should be conducted, each time changing the cyclone's speed and assessing how the current transports in the Danish Straits change.

Conclusions

The obtained results allow us to draw the following main conclusions.

1. Decomposition of sea level, atmospheric pressure, and wind fields into CEOFs revealed that during the formation and propagation of the Major Baltic Inflow in November–December 2014, the first five CEOFs describe 97% of the spatiotemporal variability of sea level and atmospheric pressure, but only 77% of the tangential wind stress. The first sea level CEOF accounts for 77% of the variance, the second CEOF contributes 10%, while the third CEOF contributes 6%. The influence of other spatial modes is insignificant. In the variability of atmospheric pressure and tangential wind stress fields, the influence of the first CEOF, although dominant, is significantly smaller compared to the sea level field, amounting to 53% and 33%, respectively.

2. Analysis of the spatial distribution of amplitudes of the first three CEOFs obtained from modeling the sea level fields of the North and Baltic Seas using the baroclinic INMOM model during MBI development showed significant inter-basin differences. In the North Sea, the main amplitude maxima of the first two modes are located in the southeastern region, while the third mode reaches its highest values in the southwest. In the Baltic Sea, the main maximum of the first mode is observed in the Gulf of Riga, and for the second and third modes – in the southwestern Baltic. The spatial distribution of phases indicates that the response of sea level fields in the North and Baltic Seas system to the impact of anemobaric forces during MBIs manifests as low-frequency wave processes demonstrating characteristics of both progressive and standing modes of wave motion.

3. The results of cross-correlation analysis of the principal components of the decomposition of atmospheric process and sea level fields into CEOFs showed that during MBIs, a high correlation (0.67) is observed only between the first principal components of sea level and atmospheric pressure. There is no correlation between all principal components of tangential wind stress and sea level field variability.

4. The wavelet analysis of the first CEOF principal components for sea level and atmospheric pressure fields revealed that in the period without an MBI (November–December 2006), the relationship between these processes was limited to the range of short-period oscillations (2–4 days), characteristic of the passage of atmospheric cyclones. However, during MBI development in 2014, the main energy exchange between the atmosphere and the ocean was observed in a lower frequency range with periods of several weeks.

5. The results of statistical data analysis demonstrate that during the MBI formation period, current spectra are characterized by a dominance of the low-frequency component (32–62 days), while shorter-period oscillations (11–14, 7, and 4 days) contribute significantly less to the total variability. Spatial analysis of the wind-current relationship showed that areas of high correlation and coherence at the main energy-carrying frequencies have a clearly expressed localization, covering only certain parts of the sea areas, which highlights the regional specificity of wind forcing on water dynamics during extreme inflow events. Such zones in the North Sea are the Skagerrak Strait, certain areas of the Norwegian Trench, the shallow southeastern and southern parts of the sea, and some areas of its northwestern and

central parts. In the Baltic Sea, similar areas are observed in the Kattegat Strait, the coastal zone of the southern part of the sea, areas of the central Baltic around Gotland Island, localized areas in the Gulf of Riga, a narrow coastal zone in the east of the Bothnian Sea, and some local areas of its central part.

6. Analysis of the synoptic situation over the North Atlantic and the results of numerical hydrodynamic modeling of free sea level oscillations in the North and Baltic Seas system showed that the largest sea level gradients between the Kattegat Strait and the southwestern Baltic, as well as the highest current velocities in the Danish Straits during the MBI, were observed on December 11, 2014, when the movement of a deep atmospheric cyclone slowed sharply to 1.0 m/s and its speed became equal to the phase velocities of free low-frequency waves in the North and Baltic Seas. This provides a basis for future verification, using numerical experiments, of the hypothesis regarding the resonant mechanism of Major Baltic Inflow generation.

REFERENCES

1. Dickson, R.R., 1973. The Prediction of Major Baltic Inflows. *Deutsche Hydrographische Zeitschrift*, 26(3), pp. 97-105. https://doi.org/10.1007/BF02232597
2. Terziev, F.S., Rozhkov, V.A. and Smirnova, A.I., eds., 1992. *Hydrometeorology and Hydrochemistry of the Seas of the USSR. Volume 3. Baltic Sea. Issue 1*. Hydrometeorological Conditions. Saint Petersburg: Gidrometeoizdat, 449 p. (in Russian).
3. Fischer, H. and Matthäus, W., 1996. The Importance of the Drogden Sill in the Sound for Major Baltic Inflows. *Journal of Marine Systems*, 9(3–4), pp. 137-157. https://doi.org/10.1016/s0924-7963(96)00046-2
4. Matthäus, W., 2006. The History of Investigation of Salt Water Inflows into the Baltic Sea – from the Early Beginning to Recent Results. In: IFO, 2006. *Meereswissenschaftliche Berichte (Marine Science Reports)*. Warnemunde: Institute Für Ostseeforschung. S. 65, 79 p. https://doi.org/10.12754/msr-2006-0065
5. Mohrolz, V., Naumann, M., Nausch, G., Krüger, S. and Gräwe, U., 2015. Fresh Oxygen for the Baltic Sea – An Exceptional Saline Inflow after a Decade of Stagnation. *Journal of Marine Systems*, 148, pp. 152-166. https://doi.org/10.1016/j.jmarsys.2015.03.005
6. Tikhonova, N.A. and Sukhachev, V.N., 2017. Wave Interpretation of Major Baltic Inflows. *Russian Meteorology and Hydrology*, 42(4), pp. 258-266. https://doi.org/10.3103/S1068373917040069
7. Zakharchuk, E.A., Litina, E.N., Klevantsov, Y.P., Sukhachev, V.P. and Tikhonova, N.A., 2017. Nonstationarity of the Hydrometeorological Processes in the Baltic Sea at Climate Changing Conditions. *Trudy GOIN*, 218, pp. 6-62.
8. Wyrtki, K., 1954. Die Dynamik der Wasserbewegungen in Fehmarnbelt II. *Kieler Meeresforschungen*, 10(2), pp. 162-181 (in German).
9. Leppäranta, M. and Myrberg, K., 2009. *Physical Oceanography of the Baltic Sea*. Springer Praxis Books. Berlin, Heidelberg: Springer, 378 p. https://doi.org/10.1007/978-3-540-79703-6
10. Madsen, K.S. and Højerslev, N.K., 2009. Long-Term Temperature and Salinity Records from the Baltic Sea Transition Zone. *Boreal Environment Research*, 14(1), pp. 125-131.
11. Zakharchuk, E.A., Sukhachev, V.N. and Tikhonova, N.A., 2024. Wave Nature and Modulation of Annual Fluctuations in the Level of the Baltic Sea. *Physical Oceanography*, 31(2), pp. 208-230.
12. Zhurbas, V., Oh, I.S. and Paka, V., 2002. Generation of Mesoscale Cyclonic Eddies in the Baltic Sea during the Inflows of the North Sea Water. *Oceanology*, 42(6), pp. 765-774.
13. Zhurbas, V.M., Oh, I.S. and Paka, V.T., 2003. Generation of Cyclonic Eddies in the Eastern Gotland Basin of the Baltic Sea Following Dense Water Inflows: Numerical Experiments. *Journal of Marine Systems*, 38(3–4), pp. 323-336. https://doi.org/10.1016/S0924-7963(02)00251-8

14. Matthäus, W. and Franck, H., 1992. Characteristics of Major Baltic Inflows – A Statistical Analysis. *Continental Shelf Research*, 12(12), pp. 1375-1400. https://doi.org/10.1016/0278-4343(92)90060-W

15. Meier, H.E.M., Döscher, R., Broman, B. and Piechura, J., 2004. The Major Baltic Inflow in January 2003 and Preconditioning by Smaller Inflows in Summer/Autumn 2002: A Model Study. *Oceanologia*, 46(4), pp. 557-579.

16. Mohrholz, V., 2018. Major Baltic Inflow Statistics – Revised. *Frontiers in Marine Science*, 5, 384. https://doi.org/10.3389/fmars.2018.00384

17. Zakharchuk, E.A., Kudryavtsev, A.S. and Sukhachev, V.N., 2014. On the Resonance-Wave Mechanism of Major Baltic Inflows. *Russian Meteorology and Hydrology*, 39(2), pp. 100-108. https://doi.org/10.3103/S1068373914020058

18. Zakharchuk, E.A., Vinogradov, M.V., Sukhachev, V.N., Tikhonova, N.A., Travkin, V.S. and Uleysky, M.Yu., 2024. Peculiarities of Variability of the Thermohaline Structure and Dynamics of the Baltic Sea Waters during the Appearance and Distribution of the Major Baltic Inflow in December 2014. *Vestnik of Saint Petersburg University. Earth Sciences*, 69(4), pp. 734-763. https://doi.org/10.21638/spbu07.2024.407 (in Russian).

19. Wyrtki, K., 1953. Die Dynamik der Wasserbewegungen in Fehmarnbelt. *Kieler Meeresforschungen*, 9(2), pp. 155-170 (in German).

20. Matthäus, W. and Franck, H., 1987. Is the Positive Salinity Anomaly in the Kattegat Deep Water a Necessary Precondition for Major Baltic Inflows. *Gerlands Beiträge zur Geohysik*, 9(4), pp. 332-343.

21. Zakharchuk, E.A. and Sukhachev, V.N., 2018. Application of Satellite Altimetry Data for Analysis of Peculiarities in Synoptic Sea-Level Perturbations Forced by Wind Stress in the Baltic Sea – the North Sea System. *Sovremennye Problemy Distantsionnogo Zondirovaniya Zemli iz Kosmosa*, 15(7), pp. 163-174. https://doi.org/10.21046/2070-7401-2018-15-7-163-174 (in Russian).

22. Pedlosky, J., 1987. *Geophysical Fluid Dynamics*. Springer-Verlag New York Berlin Heideberg, 710 p.

23. LeBlond, P.H. and Mysak, L.A., 1978. *Waves in the Ocean*. Elsevier Oceanography Series. Amsterdam; New York: Elsevier, 602 p.

24. Gräwe, U., Friedland, R. and Burchard, H., 2013. The Future of the Western Baltic Sea: Two Possible Scenarios. *Ocean Dynamics*, 63(8), pp. 901-921. https://doi.org/10.1007/s10236-013-0634-0

25. Zakharchuk, E.A., Tikhonova, N.A. and Sukhachev, V.N., 2023. Variability of the Baltic Sea Level. In: SFU, 2023. *Water Resources in the Face of Global Challenges: Environmental Issues, Management, and Monitoring: Proceedings of the Scientific and Practical Conference*. Vol. 2. Rostov-on-Don: Southern Federal University, pp. 57-62 (in Russian).

26. Golitsyn, G.S., Mokhov, I.I., Akperov, M.G., Bardin, M.Yu. and Volodin, Ye.M., 2007. Assessment of Hydrometeorological Risks and Atmospheric Vortex Intensity Distribution Functions Based on Reanalysis Data and Climate Models. *Issues of Risk Analysis*, 4(1), pp. 27-37 (in Russian).

27. Hordoir, R., Axell, L., Löptien, U., Dietze, H. and Kuznetsov, I., 2015. Influence of Sea Level Rise on the Dynamics of Salt Inflows in the Baltic Sea. *Journal of Geophysical Research: Oceans*, 120(10), pp. 6653-6668. https://doi.org/10.1002/2014JC010642

28. Pemberton, P., Löptien, U., Hordoir, R., Höglund, A., Schimanke, S., Axell, L. and Haapala, J., 2017. Sea-Ice Evaluation of NEMO-Nordic 1.0: A NEMO-LIM3.6-Based Ocean-Sea-Ice Model Setup for the North Sea and Baltic Sea. *Geoscientific Model Development*, 10(8), pp. 3105-3123. https://doi.org/10.5194/gmd-10-3105-2017

29. Zalesny, V.B., Marchuk, G.I., Agoshkov, V.I., Bagno, A.V., Gusev, A.V., Diansky, N.A., Moshonkin, S.N., Tamsalu, R. and Volodin, E.M., 2010. Numerical Simulation of Large-Scale Ocean Circulation Based on the Multicomponent Splitting Method. *Russian Journal of Numerical Analysis and Mathematical Modelling*, 25(6), pp. 581-609. https//doi.org/10.1515/RJNAMM.2010.036

30. Diansky, N.A., 2013. [*Modeling the Ocean Circulation and Study of Its Response to Short- and Long-Period Atmospheric Influences*]. Moscow: Fizmatlit, 272 p. (in Russian).

31. Brydon, D., Sun, S. and Bleck, R., 1999. A New Approximation of the Equation of State for Seawater, Suitable for Numerical Ocean Models. *Journal of Geophysical Research: Oceans*, 104(C1), pp. 1537-1540. https://doi.org/10.1029/1998JC900059

32. Yakovlev, N.G., 2009. Reproduction of the Large-Scale State of Water and Sea Ice in the Arctic Ocean in 1948–2002: Part I. Numerical Model. *Izvestiya, Atmospheric and Ocean Physics*, 45(3), pp. 357-371. https://doi.org/10.1134/S0001433809030098

33. Hunke, E.C. and Dukowicz, J.K., 1997. An Elastic-Viscous-Plastic Model for Sea Ice Dynamics. *Journal of Physical Oceanography*, 27(9), pp. 1849-1867. https://doi.org/10.1175/1520-0485(1997)027<1849:AEVPMF>2.0.CO;2

34. Hersbach, H., Bell, B., Berrisford, P., Hirahara, S., Horányi, A., Muñoz-Sabater, J., Nicolas, J., Peubey, C., Radu, R. [et al.], 2020. The ERA5 Global Reanalysis. *Quarterly Journal of the Royal Meteorological Society*, 146(730), pp. 1999-2049. https://doi.org/10.1002/qj.3803

35. Jensen, T.G., 1998. Open Boundary Conditions in Stratified Ocean Models. *Journal of Marine Systems*, 16(3–4), pp. 297-322. https://doi.org/10.1016/S0924-7963(97)00023-7

36. Manilyuk, Yu.V., Lazorenko, D.I. and Fomin, V.V., 2020. Investigation of Seiche Oscillations in the Adjacent Bays by the Example of the Sevastopol and the Quarantine Bays. *Physical Oceanography*, 27(3), pp. 242-256. https://doi.org/10.22449/1573-160X-2020-3-242-256

37. Björnsson, H. and Venegas, S.A., 1997. *A Manual for EOF and SVD Analysis of Climate Data*. CCGCR Report No. 97-1. Climate Research Branch, Environment Canada, 52 p.

38. Kolesnikova, V.N. and Monin, A.S., 1965. [On the Oscillation Spectra of Meteorological Fields]. *Ivestiya of Academy of Sciences, USSR. Atmospheric and Oceanic Physics*, 1(7), pp. 653-669 (in Russian).

39. Fennel, W. and Seifert, T., 2008. Oceanographic Processes in the Baltic Sea. *Die Küste*, 74, pp. 77-91.

40. Zakharcuk, E.A., Tikhonova, N., Zakharova, E. and Kouraev, A.V., 2021. Spatiotemporal Structure of Baltic Free Sea Level Oscillations in Barotropic and Baroclinic Conditions from Hydrodynamic Modelling. *Ocean Science*, 17(2), pp. 543-559. https://doi.org/10.5194/os-17-543-2021

41. Jönsson, B., Döös, K., Nycander, J. and Lundberg, P., 2008. Standing Waves in the Gulf of Finland and Their Relationship to the Basin-Wide Baltic Seiches. *Journal of Geophysical Research: Oceans*, 113(C3), 2006JC003862. https://doi.org/10.1029/2006JC003862

42. Kulikov, E.A. and Medvedev, I.P., 2013. Variability of the Baltic Sea Level and Floods in the Gulf of Finland. *Oceanology*, 53(2), pp. 145-151. https://doi.org/10.7868/S003015741302010X

43. Horsburgh, K., Haigh, I.D., Williams, J., De Dominicis, M., Wolf, J., Inayatillah, A. and Byrne, D., 2021. “Grey Swan” Storm Surges Pose a Greater Coastal Flood Hazard than Climate Change. *Ocean Dynamic*, 71(6–7), pp. 715-730. https://doi.org/10.1007/s10236-021-01453-0

44. Sepp, M., Post, P., Mändla, K. and Aunap, R., 2018. On Cyclones Entering the Baltic Sea Region. *Boreal Environment Research*, 23, pp. 1-14.

45. Tikhonova, N.A., Zakharchuk, E.A., Vinogradov, M.V. and Travkin, V.S., 2025. Modeling of the Major Baltic Inflow Using a Joint Model of the North and Baltic Seas. *Physical Oceanography*, 32(2), pp. 211-237.

46. Averkiev, A.S. and Klevanny, K.A., 2007. Determining Cyclone Trajectories and Velocities Leading to Extreme Sea Level Rises in the Gulf of Finland. *Russian Meteorology and Hydrology*, 32(8), pp. 514-519. https://doi.org/10.3103/S1068373907080067

47. Buchwald, V.T., 1973. Long Period Divergent Planetary Waves. *Geophysical Fluid Dynamics*, 5(1), pp. 359-367. https://doi.org/10.1080/03091927308236125

48. Byshev, V.I., 2003. *Synoptical and Large-Scale Variability of Ocean and the Atmosphere*. Moscow: Nauka, 343 p. (in Russian).

Submitted 30.10.2025; approved after review 21.11.2025;

accepted for publication 28.01.2026.

About the authors:

Evgeniy A. Zakharchuk, Head of Oceanology Department, Institute of Earth Sciences, St. Petersburg State University (33-35, 10th Line V.O., Saint Petersburg, 199178, Russian Federation), DSc. (Geogr.), **ORCID ID: 0000-0001-6079-5739**, **ResearcherID: N-1644-2013**, **Scopus Author ID: 6603158329**, **RSCI SPIN-code: 7724-4240**, eazakharchuk@yandex.ru

Natalia A. Tikhonova, Associate Professor, Oceanology Department, Institute of Earth Sciences, St. Petersburg State University (33-35, 10th Line V.O., Saint Petersburg, 199178, Russian Federation); Acting Head of Laboratory, Saint Petersburg Branch, N.N. Zubov State Oceanographic Institute (38 Bering Str., Saint Petersburg, 199397, Russian Federation), CSc. (Geogr.), **ORCID ID: 0000-0002-4546-4920**, **ResearcherID: I-4647-2015**, **Scopus Author ID: 11239410500**, **SPIN-code: 9870-7279**, i@ntikhonova.ru

Vladimir N. Sukhachev, Leading Researcher, Saint Petersburg Branch, N.N. Zubov State Oceanographic Institute (38 Bering Str., Saint Petersburg, 199397, Russian Federation); Researcher, Institute of Earth Sciences, St. Petersburg State University (33-35, 10th Line V.O., Saint Petersburg, 199178, Russian Federation), CSc. (Geogr.), **ORCID ID: 0000-0003-4821-4342**, **ResearcherID: N-7470-2015**, **Scopus Author ID: 55969236600**, **SPIN-code: 4963-7802**, syhachev@mail.ru

Contribution of the co-authors:
Evgeniy A. Zakharchuk – overall supervision of the work; drafting of the manuscript

Natalia A. Tikhonova – analysis and processing of modeling data

Vladimir N. Sukhachev – analysis and processing of atmospheric data

The authors have read and approved the final manuscript.
The authors declare that they have no conflict of interest.